Lawrence Berkeley National Laboratory
LBL Publications

Title

Land Resources for Wind Energy Development Requires Regionalized Characterizations

Permalink

Journal

ISSN

Authors

Dai, Tao

Valanarasu, Jeya Maria Jose

Zhao, Yifan

et al.

Publication Date

2024-03-19

DOI

Copyright Information

1   **Land Resources for Wind Energy Development Requires Regionalized**

2   **Characterizations**

3   Tao Dai[1,2], Jeya Maria Jose Valanarasu [3], Yifan Zhao[4], Shuwen Zheng[1], Yinong Sun[4],

4   Vishal M Patel[2], Sarah M. Jordaan[5,6,*]

5   1. School of Advanced International Studies, Johns Hopkins University, Washington, DC,

6   20036, USA

7   2. Joint BioEnergy Institute, Lawrence Berkeley National Laboratory, Emeryville, CA

8   94608, USA

9   3. Department of Electrical and Computer Engineering, Johns Hopkins University,

10   Baltimore, Maryland, 21218, USA

11   4. Department of Environmental Health and Engineering, Johns Hopkins University,

12   Baltimore, Maryland, 21218, USA

13   5. Department of Civil Engineering, McGill University, Montreal, Quebec H3A 0G4,

14   Canada

15   6. Trottier Institute of Sustainability in Engineering and Design, McGill University,

16   Montreal, Quebec H3A 0G4, Canada

17   ***Corresponding author**: Sarah M Jordaan, Ph.D.

18   **Email:** sarah.jordaan@mcgill.ca

21   **Abstract**

22   Estimates of the land area occupied by wind energy differ by orders of magnitude due to

23   data scarcity and inconsistent methodology. We developed a method that combines machine

24   learning-based imagery analysis and geographic information systems and examined the land area

25   of 318 wind farms (15,871 turbines) in the U.S. portion of the Western Interconnection. We

26   found that prior land use and human modification in the project area are critical for land-use

efficiency and land transformation of wind projects. Projects developed in areas with little human modification have a land-use efficiency of 63.8±8.9 W/m^2 (mean±95% confidence interval) and a land transformation of 0.24±0.07 m^2/MWh while values for projects in areas with high human modification are 447±49.4 W/m^2 and 0.05±0.01 m^2/MWh, respectively. We show land resources for wind can be quantified consistently with our replicable method; a method that obviates >99% of the workload using machine learning. To quantify the peripheral impact of a turbine, buffered geometry can be used as a proxy for measuring land resources and metrics when a large enough impact radius is assumed (e.g., >4 times the rotor diameter). Our analysis provides a necessary first step towards regionalized impact assessment and improved comparisons of energy alternatives.

Keywords: Wind Energy; Machine Learning; Land Use; Environmental Impact Assessment; Image Segmentation; Geographical Information System; Remote Sensing; Life Cycle Assessment.

Synopsis: Macro-energy analyses lack data inventories necessary to accurately quantify land impacts of energy. Combining machine learning, geographic information systems, and energy systems analysis, this research quantifies and maps the direct land impacts of wind power across the U.S. Western Interconnection.

Graphic for Table of Contents (TOC)
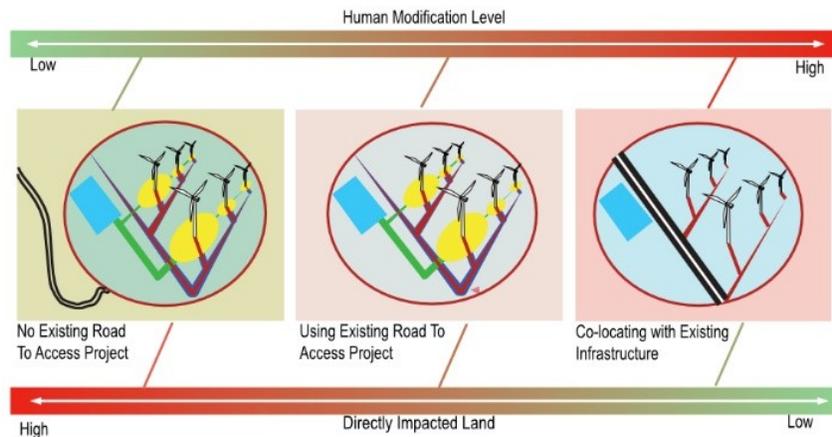
Introduction

Large-scale wind power is among the most important renewable and affordable alternatives to fossil fuels for achieving a decarbonized energy system.[1,2] Despite decarbonization benefits, the large extent of land required for the growth of wind power has been identified as a critical barrier

9

10

49 to its deployment.[3–5] Compared to other energy technologies, wind power is perceived to have a

50 relatively low capacity-based land-use efficiency (LUE), defined as the ratio of the nameplate

51 capacity of a wind farm to its land requirement in W/m^2. Recent studies on wind farms have

52 documented a capacity-based LUE of 4.3 W/m^2 (standard deviation = 3.5 W/m^2) (Harrison-Atlas

53 et al. (2022)[6]) or as low as a mean of ~2 W/m^2 (Miller and Keith (2019)[7]), an order of magnitude

54 lower than utility-scale solar PV.[8] Such estimates provide critical information for energy systems

55 planning and decisions about future energy siting. However, it is widely acknowledged that land

56 area directly impacted by wind energy development constitutes only a small fraction (typically

57 <5%) of the total project area, as wind turbines are sited to optimize electricity generation from

58 the kinetic energy of air in the free troposphere.[6,9,10] Wind farms often co-occur on landscapes

59 with other human activities, such as agriculture. When accounting only the directly impacted

60 land, LUE can be as high as 200 W/m^2.[11] The representativeness of LUE values is limited in

61 energy systems planning due to the focus on the wind farm rather than the directly impacted land

62 footprint.

63 Early studies that quantified relationship between wind energy and land in the U.S. were

64 performed at relatively smaller scale.[12,13] Extrapolating such relationships at geospatial scales was

65 therefore inappropriate and further challenged by the lack of publicly accessible project

66 information (e.g., turbine location, turbine capacity, and turbine diameter).[14] One such early and

67 foundational study examined land-wind energy interactions by assessing capacity-based LUE for

68 both "total impacted" and "directly impacted" land using data from published environmental

69 impact statements.[15] The authors defined the "total impacted" land as leased area used by the

70 entire wind farm and the "directly impacted" land as the area disturbed by the wind turbines,

71 access roads and other infrastructure.

72 More recently, the integration of imagery analysis and geographic information systems

73 (GIS) has improved the quantification of relationships between energy developments and land.

74 Geospatial methods have been used in the analyses of other energy infrastructure types[16–19] as they

75 support a better understanding of land-use and land-cover change patterns across diverse

76 geographies. Typical methods include manual delineation and geoprocessing. With manual

77 delineation, an analyst delineates the boundaries of the different elements of an energy project,

78 producing an annotated map of the directly impacted land. Diffendorfer and Compton (2014)

11

12

79 applied manual delineation and conducted a detailed examination on how land cover, topography,

80 and turbine configuration are related to the extent of land transformation.[20]

81   Geoprocessing, on the other hand, avoids the burden of mapping the directly impacted land

82 and uses automatically generated zones (e.g., circular buffered zones, minimum bounding

83 geometries and Thiessen polygons) around wind turbines as an approximation of impacted land.

84 Large scale analysis to the extent of countries is possible with this approach[21–23] but results may

85 not be accurate. Underestimation can occur when the analysis does not account for the full extent

86 of the access roads. Overestimation can occur if the analysis neglects to account for land that was

87 already developed prior to the construction of wind farms. For example, the geoprocessing

88 approach may result in overestimated LUE estimates for the two following reasons. First, the

89 buffered areas around turbines include land in use for agriculture that are not used by the turbines

90 themselves. Second, the development of wind farms in these regions use existing roads networks,

91 so the related infrastructure requires less new land (i.e., a land sparing opportunity).[24,25] While

92 results using geoprocessing suggested that the LUE of wind has been decreasing over time,[6,7]

93 Diffendorfer et al.[25] showed that new projects use existing road networks (with evidence from

94 manual delineation) and thus require less new land. Systematic categorization of wind farms

95 considering land cover type is thus needed to support a better understanding of impacts on lands

96 with and without pre-existing infrastructure developments.

97   Manual delineation can be challenging and time consuming for energy infrastructure that

98 requires a large population of facilities across extensive regions, such as wind turbines and

99 natural gas production sites, especially when using high resolution imagery. For example, a

100 previous study demonstrated that >130 hours is needed for the manual delineation of 60 km^2 of

101 land use by natural gas production, which could represent the time of manual delineation needed

102 for one wind farm, which has an median area of ~80 km^2 in the U.S.[6,26] As turbines with larger

103 rotor diameter becoming more available, future workload of manual delineation could become

104 greater as turbines needs to be spaced at a larger distance from each other. Advanced automatic

105 delineating methods present enormous potential reducing the workload of quantifying directly

106 impacted land of large-scale energy infrastructure, as shown in Dai et al. (2023), which quantifies

107 the land use of natural gas production using a machine learning-based approach and reached a

108 processing speed higher than 3.2 second/km^2.[27]

109   We introduce a novel automatic delineation approach based on computer vision and deep

110 learning (hereafter, image segmentation) to map land directly impacted by wind farms at a large

111 scale. Image segmentation is the task of assigning a pre-defined land-use class label (e.g., "Access

112 Road"), to each pixel found in an image. Image segmentation has been widely applied to land-use

113 quantification and land-cover classification, yet has primarily been used in energy studies focused

114 on solar energy development.[28–32] We combined image segmentation with GIS analysis in a

115 workflow that includes image preparation, image segmentation, and postprocessing for the

116 accurate mapping of wind energy infrastructure. Results include the capacity-based LUE and land

117 transformation (m^2/MWh). Land transformation is the ratio of land use to the life-time electricity

118 generation of a power plant and facilitates a consistent comparison of land use for wind energy

119 and other types of power generation technologies, from a life cycle perspective.[33] Our study

120 provides a transparent and practical solution for determining the land area for large-scale wind

121 energy infrastructure, extending the use of machine learning to new applications in energy

122 systems analysis. Our approach and results will be a steppingstone to regionalized environmental

123 impact assessments by providing a solid base for the evaluation of the land-use impacts in areas

124 with varying levels of human development. Such information has implications for life cycle

125 assessment (LCA)—a cradle-to-grave analysis of the environmental burdens of products and

126 processes—which mainly relies on background literature or limited inventories to quantify land

127 impacts.[34] LCA has been advancing in its capacity to incorporate spatiotemporal information into

128 environmental impact methods for land,[35,36] which have been challenged by the lack of spatially

129 explicit inventories.[37,38] More recently, a life cycle inventory for all power plants in the United

130 States has been developed; yet, spatially explicit land-use data remains limited.[39,40] Impact

131 assessments for wind energy development on ecosystems, landscape, and ecosystem services also

132 require spatially explicit data and high resolution maps.[41,42,43,44] Results here are presented in terms

133 of LUE (W/m2) but also provided in a format for broader applicability that includes energy

134 systems planning and LCA.

135 **Materials and Methods**

136 **Study Area and Data Sources.** Our study area is the U.S. part of the Western Interconnection

137 (Figure 1a).[45,46] Wind turbine locations and attributes were sourced from the US Wind Turbine

138 Database,[14] and projects that were constructed between 1981 and 2018 were included in this

139 study. Aerial imageries with a resolution of 1 meter or less acquired in 2018 from the National

Agriculture Imagery Program (NAIP) are used when applicable, and images from 2017 or 2019 when required since NAIP are typically collected every other year (image sources are documented in Supporting Data).
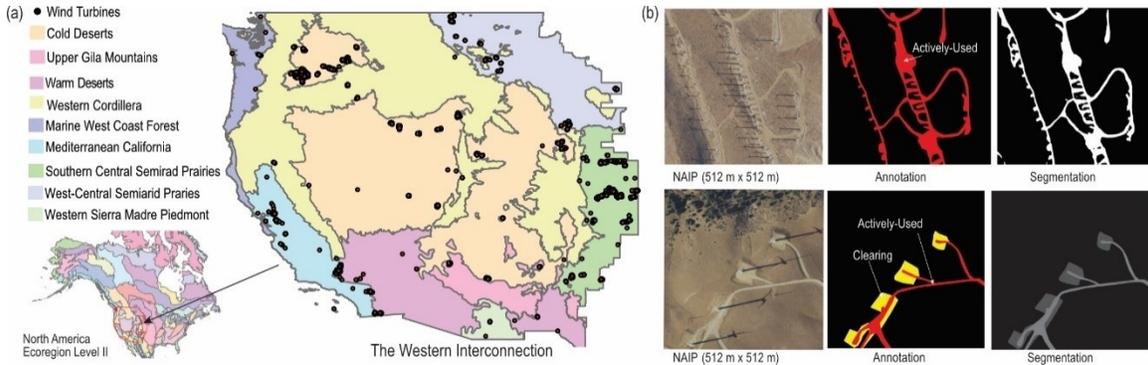
Figure 1. (a) Wind turbines in the U.S. portion of the Western Interconnection are located across a variety of ecoregions and show geographical variations of landforms (b) Annotation approach and the temporal variation of both turbine size and turbine spacing for two different projects: Directly-impacted land for older projects constructed before January 2003 (upper images) is segmented using a two-class scheme (i.e., background and actively-used), whereas for newer projects constructed after December 2002 (lower images), we used a three-class scheme (background, actively-used, and regenerating).

The main infrastructure elements of wind energy development include access roads, service roads, a circular surface land clearing for turbine installation, roadside clearing, and surface land clearing for buried cable. We simplify and categorize the land requirement by wind energy infrastructure into three classes, i.e., background, actively-used, and regenerating, based on their land occupation characteristics and visual appearance on imagery (Figure 1b). The background class is area not directly impacted by wind farm construction. The actively-used class includes access roads and service roads that shows a bright and smooth texture in an imagery. The regenerating class may include temporary roads, roadside clearings, temporary storage and laydown areas, land use by buried cable, and the circular clearing, which show a dim and rough texture in imagery. For older projects (typically before January 2003 in the WECC), we assume that the regenerating class has fully reclaimed and thus we use a two-class scheme (i.e., background and actively-used).

The workflow to determine land use via imagery segmentation includes three steps: deep learning model development, deep learning model application, and postprocessing.

Deep Learning Model Development. This step includes training set preparation, model training, and model validation. The images in the training set are discretely sampled according to the

166   turbine locations across the study area to allow the deep learning model to recognize the various

167   landscapes among wind projects. The training set was manually delineated in ArcGIS Pro

168   supported by turbine location information from the USGS Wind Turbine Database. The manual

169   recognition of NAIP pixel classes (e.g., whether a pixel should be categorized as background,

170   actively-used, or regenerating) was aided by the reference world topographic map and world hill

171   shade map in ArcGIS Pro.[47] In challenging landscapes, experts in the Expert Review Panel (see

172   Acknowledgement) were consulted to ensure accuracy and quality. The training set preparation

173   process and the delineation results were presented to the Expert Review Panel to guarantee the

174   quality of the training set. >90% of the delineation was completed by the first author to ensure

175   consistency using the quality assurance noted above. Detailed process of creating the training set

176   can be found at Supplementary Note 1.

177   A dense version of U-Net network is used for training our model, which is an "encoder-

178   decoder" type of architecture where the input image is translated to a low dimensional latent

179   space using the encoder and then the decoder takes back the latent space to the image space to

180   output the segmentation mask.[48] The encoder and decoder of the network consist of five blocks

181   and each block consists of a dense convolutional block followed by batch normalization and

182   ReLU non-linearity (Figure S1). U-Net is one of the most widely used deep-learning frameworks

183   for image segmentation and has showed state-of-the art performance compared to its followers, as

184   shown in recent studies in a variety of areas, including land-cover mapping.[49–52] There are max-

185   pooling layers after each subsequent encoder block and upsampling layers after each subsequent

186   decoder block. For upsampling, a simple bilinear interpolation operation is employed. The output

187   segmentation mask is trained by supervising it with a cross-entropy loss over the ground truth.

188   The network is trained for 400 epochs using Adam optimizer and a learning rate of 0.001. The

189   network is developed and trained using the PyTorch framework on an NVIDIA RTX 8000

190   GPU. Notably, the following geographical processing is independent on the selection of deep

191   learning method, so our framework is flexible to incorporate other image segmentation

192   approaches.

193   We trained two separate dense U-Net models: one old project model and a new project

194   model due to their differences in turbine size, turbine configuration, and vegetation reclaiming

195   status. The old project model is trained on 301 images and their annotations (25 test images). The

196   new project model is trained on 1687 images (75 test images). For validation, we separate the test

29

30

197 data, which consists of manual annotations and are not part of the training dataset. The model

198 performance is evaluated based on F1 score, which is defined as:

199
$$F1 = \frac{2\,TP}{2\,TP + FN + FP}$$
(1)

200 where TP, FN, and FP correspond to the number of true positives (i.e., correctly classified), false

201 negatives (i.e., wrongly classified as another class), and false positives (i.e., wrongly classified

202 from another class to the current class) in the output prediction, respectively. Detailed description

203 of our model training can be found at Supplementary Note 2.

204 Model application and postprocessing are conducted on a cluster basis, with each cluster formed

205 by a predefined minimum number of turbines, N_t, that are located within a search distance, d_s

206 (Supplementary Note 3 provides further detail).

207 **Energy Systems Analysis.** We calculated the capacity-based LUE and land transformation of the

208 selected projects based on the annual net generation from the U.S. Energy Information

209 Administration and the USGS Wind Turbine Database (Version 3.0.1). As a variety of metrics

210 have been used in energy systems analysis,[53,54] we selected capacity-based LUE and land

211 transformation based on their frequency and acceptance of usage on comparative assessments of

212 energy technologies and life cycle assessments.[55,56]

213 We use the EIA-860[57] and EIA-923[58] to identify the capacity factor of the wind turbines

214 within the U.S. Wind Turbine Database. The capacity factor is the ratio of the actual amount of

215 electricity generation to capacity-based generation. First year data has been neglected as turbines

216 are usually not running steady in this period.[59] For turbines with missing turbine year or missing

217 turbine capacity in the U.S. Wind Turbine Database, we assigned them with project averaged

218 values. Projects with missing turbine information are listed in Supporting Data. Results from

219 Hamilton et al. (2020) on the temporal trend of capacity factor were used when electricity

220 generation data are not available from the EIA files.[59] A turbine lifetime of 30 years is assumed.

221 We compare capacity-based LUE among projects under three types of land-use

222 circumstances: 1) the initial, which includes all the original construction land uses, 2) the

223 reference-year (i.e., 2018), which represents the identified directly impacted area using the

224 marchine-learning approach, and 3) the actively-used (or "permanent land use"), which includes

31 8

32

only the land impacted by the actively used class and represents a scenario that the vegetation reclaiming process is completed. These three circumstances represent the reclamation process of the disturbance by project construction. We use results from the reference-year circumstance for agricultural projects and the initial circumstance results for other projects to compare the land transformation among projects for consistency considering the variation of project ages. The initial land use was obtained by adjusting the reference year land use to initial land use by applying the averaged measurements of the area of initial circular clearing, roadside clearing width, and width of clearing for buried cable.

Description of direct land use. Existing studies have focused on how the LUE of wind energy projects changes with variations in wind power project attributes, such as turbine capacity and year. However, we argue that to consistently identify patterns of LUE among wind farms, it is important to first limit the scope of the study to projects located at a comparable level of human modification due to the large variations in the composition of land-use elements. We limit our analysis to the core area of wind farms located in non-agricultural areas. The core area is defined as the area where turbines are connected by service roads but excluding the main access road.

240   We propose a site-residue model to describe the patterns of directly impacted land within

241   the core area. This model decomposes the directly impacted land into two parts: the sites and the

242   residues (Figure 2). The sites are assumed as linearly stacked and evenly distributed, forming into

243   a single string. The area of such a string of sites can be estimated as a function of the turbine

244   capacity. The difference between the real impacted area and the estimated impacted area between

245   every two neighboring sites is defined as a residue. For example, for a wind project with parallel

246   string configuration, the distance between strings of turbines is usually larger than twice the

247   turbine spacing. In cluster configuration, multiple service roads are often observed. Further details

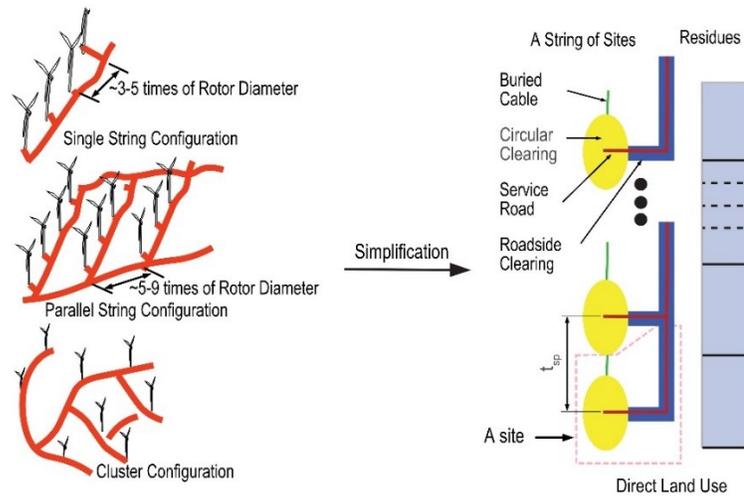248   on the model are documented in Supplementary Note 4.

249

250   Figure 2. Directly impacted land by wind farms can be described as a combination of sites and
251   residues.

252   **The outreach impact of the turbines.** We mapped and quantified the directly impacted land and

253   the occupancy of surface land. However, the noise and visual impacts of turbines are not

254   negligible, as the turbine diameter is greater than that of the circular clearing area. Researchers

255   focused on energy systems planning have applied a buffer distance from 300 meters to 1,000

256   meters to quantify this effect, as summarized by Harrison-Atlas et al. (2022).[6] For large-scale

257   studies, existing estimates also applied a universal buffer distance for all turbine sizes for

258   convenience, regardless of the turbine diameter. Here, we examine the outreach impact of

259   turbines by creating a buffer geometry extending from the directly impacted land that we

260   determined using the deep learning approach. First, a circular buffer area is created around the

261   turbine with a buffer distance from 1 to 10 times (step = 0.2) of the turbine diameter. Clusters of

262   turbines without a valid rotor diameter in the USGS Wind Turbine Database were excluded from

41

42

263   the analysis. The buffered geometry is then dissolved into the directly impacted land. This

264   dissolving process merged the polygons from both the directly impacted land and the buffered

265   geometry into a single polygon. We then calculated how the dissolve process impact the metrics

266   by calculating the relative error of area $\left(RE_A\right)$ and relative error of LUE (RE_{LUE}¿, as follows:

267   $$\Re_A = \frac{A_{dissovled} - A_{buffer}}{A_{dissolved}}$$

268   $$\Re_{LUE} = \frac{LUE_{buffer} - LUE_{dissolved}}{LUE_{dissolved}}$$

269   where $A_{dissolved}$ and $LUE_{dissolved}$ are the area and LUE calculated from the dissolved polygon,

270   respectively; and A_{buffer} and LUE_{buffer} are the area and LUE calculated from the buffered

271   geometry around wind turbines, respectively.

272   **Results and Discussions**

273   **Mapping of Directly Impacted Land by Wind Power Development.** Our framework combines

274   imagery analysis with machine learning to support efficient and accurate large-scale land-use

275   mapping of wind energy infrastructure. We mapped the directly impacted land of more than 300

276   wind farms (>15,000 Turbines) in the U.S. part of the Western Interconnection by processing

277   >90,000 images with an average processing speed of ~1.85 seconds/image, and where each image

278   represents an area from ~1.05 km^2 to ~0.26 km^2 (imagery resolution 1- 0.5 m, respectively) (Table

279   S1).

280   Our workflow achieved at least 99% accuracy in quantifying the area of directly impacted

281   land without manual delineation. By segmenting the imagery into background and directly

282   impacted land, the deep learning models identify the directly impacted land from background

283   land cover with a median background F1 score of 99.6% for old projects and 99.8% for new

284   projects (i.e., demonstrating high performance). The median F1 score for the three-class

285   classification scheme (i.e., background, actively-used, and regenerating) is 96.4% for the clearing

286   class and 96.2% for the actively-used class. The classification error mainly came from the

287   actively-used class being classified as background class (Figure S6).

288   The machine learning model substantially reduces the time and effort required for

289   obtaining the directly impacted land for wind farms. By employing machine learning, >99%

290   workload has been reduced compared to manual delineation since our model correctly identified

43   11

44

291 the majority of areas of interest, especially for the entire road network, and the remaining <1%

292 workload is related to identifying false negatives and false positives (e.g., making up the circular

293 clearing and removing noise in background). Due to the common existence of colocation in wind

294 farms, manual delineation is and will be a general required step to obtain the directly impacted

295 land for solving tasks of differentiating the purposes of land with the same land use class. For

296 example, a machine learning model can extract all the road pixels for a wind power project

297 located in agricultural area but determining which roads are used by a wind farm needs human

298 determination. The accuracy of automatic classification is critical for obtaining final results

299 efficiently since processing inaccurate automated extraction results costs more time compared to

300 pure manual processing. Compared to processing imagery with a similar resolution with an area

301 over 64 km^2, our approach uses only 0.2% to 1.6% of the time required for the existing

302 commercial automated extraction tools.[26]

303 **Characteristics of Land Use in Wind Farms**. Based on the human modification level in the

304 project area, we categorized the wind farms into four types: Access Road, No Access Road,

305 Agricultural Area, and Mixed, to show how a different configuration of land-use elements

306 impacts the performance of LUE (Figure 3a and Figure S2-S5). An Access Road project, located

307 in an area with minor human disturbances, requries the construction of an access road to connect

308 the wind farm region with existing road network. An access road is not required for the No

309 Access Road projects since they utilize existing road. Agricultural Area projects are entirely or

310 partially situated within agricultural production areas, where most of the land has been modified

311 by human activities. Mixed projects are a mix of old and new wind farms in the same area. Since

312 the turbine size in old projects is much smaller (~1/3 in terms of rotor diameter), only part of the

313 existing infrastructures can be utilized for the construction of new wind farms. Service roads and

314 circular clearings are usually still required to construct the new projects.

315

316
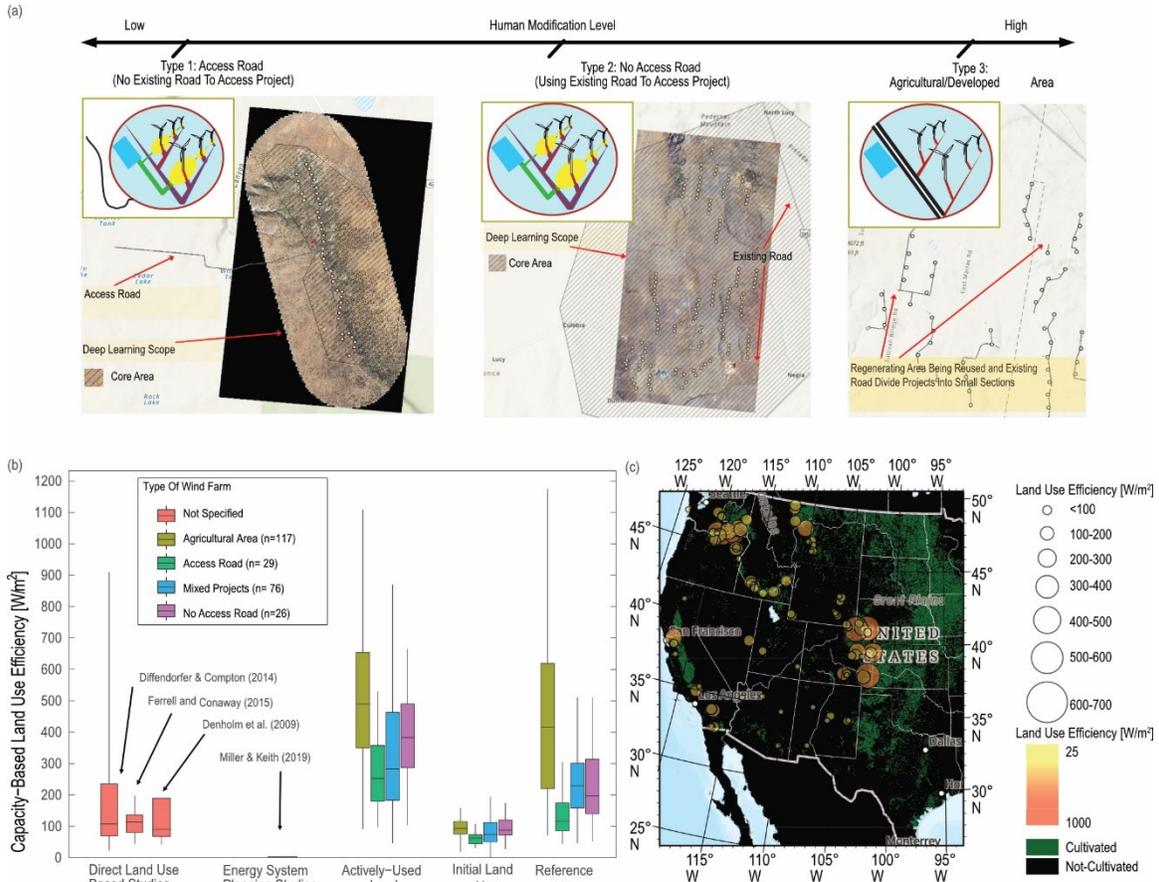
Figure 3. (a) Three types of wind farms based on the level of human modification in the project area. (b) The distribution of capacity based LUE. "Mixed Projects" are a mixed of new projects and old projects in the same area. "Actively-Used Land" represents a scenario with only actively-used class being occupied and all regenerating class are reclaimed. "Initial Land Use" is a scenario where all the initial disturbances are considered. "Reference Year" considers land use in the reference year of this study (2018) (c) The spatial distribution of LUE in the Western Interconnection.

Our results reveal that the key to improve the capacity-based LUE is to utilize existing roads (Figure 4b). In all three circumstances, Access Road projects have the lowest capacity-based LUE (a mean of 63.8 with 95% confidence interval of $\pm$8.9 W/m^2 in initial circumstance and 275$\pm$43.6 W/m^2 in actively-used circumstance). Access roads can account for up to ~70% and a mean of ~25% of the total road length for the Access Road projects. Being able to share access/service roads with agricultural production activities, the Agricultural Area projects have a capacity-based LUE of 95.5$\pm$ 6.0 W/m^2 under the initial circumstance, which is comparable to the No Access Road type and the Mixed type (98.7$\pm$17.9 W/m^2 and 80.4$\pm$9.8 W/m^2, respectively). Benefited from the capability of reusing a majority of the disturbed land (e.g., the circular clearing and land above buried cables), the capacity-based LUE of the Agricultural Area

type in the reference-year circumstance achieves 447 ± 49.4 W/m^2, close to their actively-used circumstance (517 ± 44.5 W/m^2). Another reason for the high LUE of the Agricultural Area type is that the service road can be very short and connects only 1-2 turbines. The capacity-based LUE of Mixed type is 80.4 ± 9.8 W/m^2 in the initial circumstance and rises to 256 ± 34.7W/m^2 in the reference-year circumstance. The increase can be attributed to the fully reclaimation of land for projects built before 2003.

Similarly, our results show that the projects of the Mixed type and the Access Road type have higher land transformation (0.27 ± 0.06 m^2/MWh and 0.24 ± 0.07 m^2/MWh, respectively). While the higher land transformation of Access Road type is from its higher initial land use, compared to No Access Road which has a land transformation of 0.16 ± 0.05 m^2/MWh), the land transformation of Mixed type (0.28 ± 0.04 m^2/MWh) is driven by their low lifetime generation. This may be because of the Mixed projects' low capacity factor due to the existence of the older models of turbines. The Mixed type also has a higher variation in land transformation, with the medium land transformation lower than the Access Road type. Wind farms in agricultural area, as expected, have the lowest land transformation at 0.05 ± 0.01 m^2/MWh.

The range of our results for capacity-based LUE are consistent with the results of the previous manual delineation studies (e.g., Diffendorfer and Compton (2014)[20] and Ferrel and Conaway (2015)[11]) and the Mixed type with a majority of projects built before 2003 shows consistency with the estimation of Denholm et al. (2009)[15]. Estimates using a geoprocessing-based approach, however, could be significantly lower, to ~2.8 W/m^2, which is due to the directly impacted land in our study is only portion of the zones (e.g., the Theissen polygons or circular buffered areas). .

It should be noted that, although we mapped the directly impacted land for 132 Agricultural Area projects, 84 Mixed projects, 50 Access Road projects, and 39 No Access Road projects, metrics can only be calculated for a portion of the projects when the required data (e.g., turbine capacity) are available.

Understanding the Variability in the Directly Impacted Land. Our results suggest that the LUE of wind farms is positively coupled with turbine capacity and is related to the number of turbines in a farm. Area of a site, as defined in Figure 2, is mainly related to two factors: turbine spacing and the radius of circular clearing. Estimation of minimum turbine spacing (Eq. S9 and Eq. S10) suggests that existing turbines are not necessarily spaced at the optimum suggested distance (Figure S12a). Circular clearing is less dependent on turbine rotor diameter and has a smaller variation compared to turbine spacing. The relationships with other land-use elements can be regarded as minor. As a result, under current wind project configurations, the increase of turbine capacity is higher than the increase of the site area, which leads to the increase of LUE as turbine rotor diameter increases.

When accounting for the residues, we found that as turbine capacity increases, both the area of residues and the proportion of site area out of total area increases. Therefore, for projects with a fixed number of turbines, the LUE increases as turbine capacity increases (Eq. S8). For projects with turbines of a capacity less than 0.5 MW, the residue area is ~200% the site area. For wind farms built before 2003, the turbine spacing can be barely larger than the rotor diameters and there are circumstances where the service roads do not connect two turbines directly but instead form a "claw" shape, which increases the total residue area. When turbines are larger than 1.5 MW, the residue area remains steady, and the site area increases as to the turbine spacing increases (Figure S12b). This could be due to the service road length per turbine nearing the distance between turbines, resulting in a reduced fraction of additional service road needed (Figure S7). The area of several sites exhibits a decline for projects using turbines with a capacity >3 MW as these turbines are located closer than those with smaller capacities (Figure S12a).

We observed that projects with a small number of wind turbines (<6 typically) have a much higher LUE as turbines in such projects can form a single line of sites. As the number of turbines increases, an increasing residue area is often required to form multiple lines of turbines (e.g., a parallel configuration). So, for projects with a fixed turbine capacity, it is reasonable to assume that, as the number of turbines increases, the ratio of the site area to the residue area is constant or decreases, which can thus lead to a decrease in LUE. However, we did not see this trend. Projects with similar turbine capacity appear to have a similar LUE as the project capacity increase (Figure S12c). One potential reason is that as the number of turbines increases, the ratio of turbine spacing to turbine rotor diameter decreases (Figure S8).

390 **Parametric buffer analysis and rotor diameter.** By parametrically increasing the buffer

391 distance surrounding the turbine, the margin of error of LUE based on buffering geometry

392 diminishes exponentially (Figure 4a). When the buffer factor exceeds four, the discrepancy

393 between both RE_A and RE_{LUE} falls below 5% for all projects. When employing methods that

394 rely on buffering geometry to quantify LUE, large errors arise for wind farms located in areas

395 with little human modification due to the larger amount directly impacted land (e.g., the

396 additional land use by the access roads).

397 With increasing buffer distance, the directly impacted area becomes inconsequential due to two

398 factors. First, the buffered geometry completely covers the directly impacted land (i.e., the

399 circular clearing and service roads are dissolved into the geometry). Second, the magnitude of

400 land-use components is minuscule in comparison to the buffer diameter. Manual measurements

401 indicate that the width of service roads, roadside clearings, and cable remains relatively

402 diminutive and consistent among projects, with maximum magnitudes not exceeding 15 meters,

403 18 meters, and 17 meters, respectively. Conversely, the magnitude of turbine diameter can be an

404 order of magnitude greater for larger turbines. Regardless, specific land uses, such as agriculture,

405 occur right up to the base of the turbine, rendering the buffer a meaningless proxy for specific

406 impacts.

65

66

407
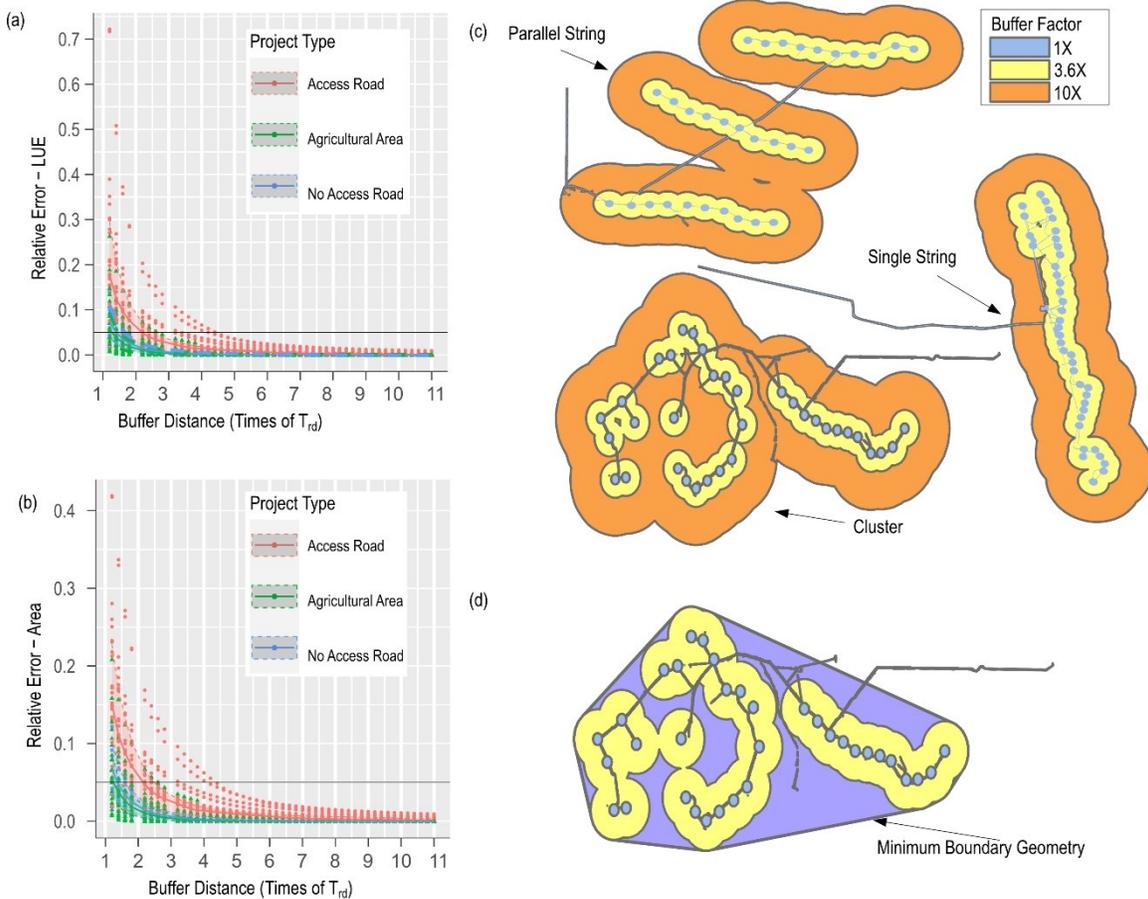
Figure 4. (a) The changes of the relative error of land use efficiency (LUE) with buffer distance (b) The changes of the relative error of area with buffer distance (c) Impact of buffer distance on the impacted area for different wind turbine configurations (d) Minimum bounding geometry could be applied for estimating land use when the turbine impact is considered as small to fill the holes in the impacted area.

Furthermore, the accuracy of buffer-based methodologies is contingent upon the configuration of the turbines (Figure 4). For a smaller buffering factor (e.g., 1X), there is an absence of overlap among the buffered geometry, rendering the geometry unsuitable for evaluating the land-use impact, except in instances where the gaps between turbines are occupied by pre-existing infrastructure, such as in developed or agricultural areas. For single string and parallel string configurations, as buffering factor increases, the buffered geometry overlaps and dissolves (Figure 4c). Service roads are dissolved into the buffer-based geometry and only a minuscule fraction of the area is excluded from these areas. In such cases, the land-use area serves as an adequate proxy for directly impacted land.

67   17

68

For projects with a cluster configuration, when the buffering factor is not large enough, additional analysis may be necessary, as additional gaps or holes can be generated within the impacted areas (Figure 4c). Another option for obtaining the amount of land-use is to create a minimum bounding convex polygon (Figure 4d), as have been applied in previous studies in energy system planning oriented studies.[43] The minimum bounding geometry is dependent on the configuration of projects and includes all of the area between turbines. However, a large fraction of undisturbed land (e.g., the purple pixels in Figure 4d) is likely to be included with a convex polygon approach. The magnitude of error could increase when the buffering distance increases.

The buffering distance and the configuration of turbines are thus critical factors to accurately assess the land-use impact of an existing wind farm. If the regionalized impact from a turbine is considered as small (e.g., <4 times of rotor diameter), it is important to obtain the directly impacted land to avoid overestimating the land-use impact in areas with high levels of human modification and to avoid underestimating it in areas with low levels of human modification. Further analysis on the uncertainty of our method is documented in Supplementary Note 5.

Future Research and Contribution

The workflow we developed can serve as a prototype for mapping the land use of wind farms in other regions and other types of energy projects. The current workflow involves manual delineation work in both training set preparation and post processing (Table S2). We chose manual processing to solve the challenges associated with co-location of wind power and other human activities. In addition, we opted for manual processing because our primary goal is achieving accurate land-use mapping. The current model helped mitigate the majority of workload. Although the deep learning model can be potentially improved by adding new annotated images, there is a tradeoff between model performance and overall time consumption. Limited by resource and time, the performance of the existing model could be inadequate for land-cover types that are beyond the geographical scope (i.e., the WECC). In such a case, our post-processed results can be used as an additional training set. Region-specified training set can also be obtained based on the documented steps in Supplementary Note 1. Similar to wind turbines, oil/natural gas production wells/pads are also dispersedly distributed across landscape, and due to the longer history and >2 orders larger number of facilities, automated approaches are

452 in demand for quantifying land use by oil/natural gas production to understand the landscape

453 consequences as manual delineation is still a main approach for land use quantification.[27,60,61] Due

454 to the dearth of data, natural gas infrastructure is generally compared to the entire wind farm in

455 planning studies, rather than solely the infrastructure for wind.[62] The utilization of these values

456 yields incommensurable results, potentially misleading decision-makers. This research fills a

457 much-needed gap in LCA and planning inventories that will enable more robust examination of

458 new and developing impact assessment methods.

459   The significance of this study lies in its introduction of an approach that enables spatially

460 explicit, empirical measurement of the direct land impacted by wind power at a large scale. The

461 analysis utilizes a machine learning approach to enable the development of data inventories

462 critical to the analysis of large-scale and regional impacts of wind development; for example,

463 such inventories have not ever before been developed for use in life cycle assessment and

464 planning studies. Importantly, we have also defined the key concepts and impact factors involved

465 in identifying patterns of land-use by wind energy. Combined with recent studies,[27] results set the

466 stage for the first consistent comparisons on environmental sustainability across different energy

467 technologies, whether in the context of LCA, environmental impact analysis or energy systems

468 planning for net zero emissions.

469 **Supporting Information**

470   Additional results, methodology description, and supplementary notes are documented in

471 Supporting Information.docx.

472   Wind farms with missing turbine information, classification of wind farms, image sources,

473 land transformation, and land use efficiency are documented in Supporting Data.xlsx.

474 Postprocessed results at a cluster level are stored at supporting_map.gdb.

475 **Author Information**

476 **Corresponding author**

477   Sarah M Jordaan, Ph.D. – McGill University, Montreal QC, H3A 1E3, Canada

478   **Email:** sarah.jordaan@mcgill.ca

479 **Authors**

77

78

480   Tao Dai - School of Advanced International Studies, Johns Hopkins University,
481   Washington, DC, 20036, USA; Joint BioEnergy Institute, Lawrence Berkeley National
482   Laboratory, Emeryville, CA 94608, USA

483   Jeya M Jose - Department of Electrical and Computer Engineering, Johns Hopkins
484   University, Baltimore, Maryland, 21218, USA

485   Yifan Zhao - Department of Environmental Health and Engineering, Johns Hopkins
486   University, Baltimore, Maryland, 21218, USA

487   Shuwen Zheng- Department of Electrical and Computer Engineering, Johns Hopkins
488   University, Baltimore, Maryland, 21218, USA

489   Yinong Sun - Department of Environmental Health and Engineering, Johns Hopkins
490   University, Baltimore, Maryland, 21218, USA

491   Vishal M Patel - Department of Electrical and Computer Engineering, Johns Hopkins
492   University, Baltimore, Maryland, 21218, USA

493   **Author Contributions:** TD, JMJ, VMP, and SMJ designed the research, TD and JMJ performed
494   research, TD and JMJ contributed new reagents/analytic tools, TD analyzed data, TD, JMJ and
495   SMJ wrote the paper.

Data Availability. Manually annotated images will be shared upon request.

References

(1) Jenkins, J. D.; Mayfield, E. N.; Larson, E. D.; Pacala, S. W.; Greig, C. Mission Net-Zero America: The Nation-Building Path to a Prosperous, Net-Zero Emissions Economy. *Joule* **2021**, *5* (11), 2755–2761.

(2) Wang, F.; Harindintwali, J. D.; Yuan, Z.; Wang, M.; Wang, F.; Li, S.; Yin, Z.; Huang, L.; Fu, Y.; Li, L. Technologies and Perspectives for Achieving Carbon Neutrality. *Innov.* **2021**, *2* (4), 100180.

(3) U.S. Energy Information Administration. Annual Energy Outlook 2022 https://www.eia.gov/outlooks/aeo/ (accessed Dec 31, 2021).

(4) Baker, S. E.; Stolaroff, J. K.; Peridas, G.; Pang, S. H.; Goldstein, H. M.; Lucci, F. R.; Colin, M. *Getting to Neutral. Options for Negative Carbon Emissions in California*; 2020.

(5) Madhu, K.; Pauliuk, S.; Dhathri, S.; Creutzig, F. Understanding Environmental Trade-Offs and Resource Demand of Direct Air Capture Technologies through Comparative Life-Cycle Assessment. *Nat. Energy* **2021**, *6* (11), 1035–1044. https://doi.org/10.1038/s41560-021-00922-6.

(6) Harrison-Atlas, D.; Lopez, A.; Lantz, E. Dynamic Land Use Implications of Rapidly Expanding and Evolving Wind Power Deployment. *Environ. Res. Lett.* **2022**, *17* (4), 044064. https://doi.org/10.1088/1748-9326/ac5f2c.

(7) Miller, L. M.; Keith, D. W. Addendum: Observation-Based Solar and Wind Power Capacity Factors and Power Densities (Environ. Res. Lett. (2018) 13 (104008) DOI: 10.1088/1748-9326/Aae102). *Environ. Res. Lett.* **2019**, *14* (7). https://doi.org/10.1088/1748-9326/ab12a2.

85

86

(8) Bolinger, M.; Bolinger, G. Land Requirements for Utility-Scale PV: An Empirical Update on Power and Energy Density. *IEEE J. Photovoltaics* **2022**, *12* (2), 589–594. https://doi.org/10.1109/JPHOTOV.2021.3136805.

(9) Mai, T.; Wiser, R.; Sandor, D.; Brinkman, G.; Heath, G.; Denholm, P.; Hostick, D. J.; Darghouth, N.; Schlosser, A. Strzepek, K. *Renewable Electricity Futures Study: Exploration of High-Penetration Renewable Electricity Futures*; Golden, CO, 2012; Vol. 1.

(10) Lovering, J.; Swain, M.; Blomqvist, L.; Hernandez, R. R. Land-Use Intensity of Electricity Production and Tomorrow's Energy Landscape. *PLoS One* **2022**, *17* (7 July), 1–17. https://doi.org/10.1371/journal.pone.0270155.

(11) Ferrell, S. L.; Conaway, J. *Wind Energy Industry Impacts in Oklahoma*; 2015.

(12) Strickland, D.; Johnson, D. Overview of What We Know About Avian/Wind Interaction. In *National Wind Coordinating Collaborative Wildlife Workgroup Research Meeting VI*; 2006.

(13) Bureau of Land Management. *Final Programmatic Environmental Impact Statement on Wind Energy Development on BLM Administered Land in the Western United States*; 2005.

(14) Rand, J. T.; Kramer, L. A.; Garrity, C. P.; Hoen, B. D.; Diffendorfer, J. E.; Hunt, H. E.; Spears, M. A Continuously Updated, Geospatially Rectified Database of Utility-Scale Wind Turbines in the United States. *Sci. Data* **2020**, *7* (1), 1–12. https://doi.org/10.1038/s41597-020-0353-6.

(15) Denholm, P.; Hand, M.; Jackson, M.; Ong, S. *Land Use Requirements of Modern Wind Power Plants in the United States*; 2009; Vol. Technical. https://doi.org/10.2172/964608.

(16) Walker, B. L.; Neubaum, M. A.; Goforth, S. R.; Flenner, M. M. Quantifying Habitat Loss and Modification from Recent Expansion of Energy Infrastructure in an Isolated, Peripheral Greater Sage-Grouse Population. *J. Environ. Manage.* **2020**, *255*. https://doi.org/10.1016/j.jenvman.2019.109819.

(17) Johnson, N. *Pennsylvania Energy Impacts Assessment. Report 1: Marcellus Shale Natural Gas and Wind*; 2010.

(18) Milheim, L. E.; Slonecker, E. T.; Roig-Silva, C. M.; Malizia, A. R. *Landscape Consequences of Natural Gas Extraction in Lackawanna and Wayne Counties, Pennsylvania, 2004-2010: U.S. Geological Survey Open-File Report 2013-1227, 32 P.*; Reston, Virginia, 2013.

(19) Milheim, L. E.; Slonecker, E. T.; Roig-Silva, C. M.; Malizia, A. R. *Landscape Consequences of Natural Gas Extraction in Lackawanna and Wayne Counties Open-File Report 2013-1227*; 2004.

(20) Diffendorfer, J. E.; Compton, R. W. Land Cover and Topography Affect the Land Transformation Caused by Wind Facilities. *PLoS One* **2014**, *9* (2). https://doi.org/10.1371/journal.pone.0088914.

(21) Murray, A. G.; Mills, B. F. Read the Label! Energy Star Appliance Label Awareness and Uptake among U.S. Consumers. *Energy Econ.* **2011**, *33* (6), 1103–1110. https://doi.org/10.1016/j.eneco.2011.04.013.

(22) Lopez, A.; Roberts, B.; Heimiller, D.; Blair, N.; Porro, G. U.S. Renewable Energy Technical Potentials: A GIS-Based Analysis. *Natl. Renew. Energy Lab. Doc.* **2012**, *1* (7), 1–40.

87

88

89

90

568 (23) Lopez, A.; Mai, T.; Lantz, E.; Harrison-Atlas, D.; Williams, T.; Maclaurin, G. Land Use and
569   Turbine Technology Influences on Wind Potential in the United States. *Energy* **2021**, *223*, 120044.
570   https://doi.org/10.1016/j.energy.2021.120044.

571 (24) Lopez, A.; Cole, W.; Sergi, B.; Levine, A.; Carey, J.; Mangan, C.; Mai, T.; Williams, T.; Pinchuk,
572   P.; Gu, J. Impact of Siting Ordinances on Land Availability for Wind and Solar Development. *Nat.*
573   *Energy* **2023**. https://doi.org/10.1038/s41560-023-01319-3.

574 (25) Diffendorfer, J. E.; Dorning, M. A.; Keen, J. R.; Kramer, L. A.; Taylor, R. V. Geographic Context
575   Affects the Landscape Change and Fragmentation Caused by Wind Energy Facilities. *PeerJ* **2019**,
576   *2019* (7). https://doi.org/10.7717/peerj.7129.

577 (26) Germaine, S. S.; O'donnell, M.; Aldridge, C. L.; Baer, L.; Fancher, T.; Mcbeth, J.; Mcdougal, R.
578   R.; Waltermire, R.; Bowen, Z. H.; Diffendorfer, J.; Garman, S.; Hanson, L. *Mapping Surface*
579   *Disturbance of Energy-Related Infrastructure in Southwest Wyoming-An Assessment of Methods*;
580   Reston, Virginia, 2012.

581 (27) Dai, T.; Valanarasu, J. M. J.; Patel, V. M.; Jordaan, S. M. The Life Cycle Land Use of Natural Gas-
582   Fired Electricity in the US Western Interconnection. *Environ. Sci. Adv.* **2023**, 815–826.
583   https://doi.org/10.1039/d3va00038a.

584 (28) Campos-Taberner, M.; García-Haro, F. J.; Martínez, B.; Izquierdo-Verdiguier, E.; Atzberger, C.;
585   Camps-Valls, G.; María, &; Gilabert, A. Understanding Deep Learning in Land Use Classification
586   Based on Sentinel-2 Time Series. **2020**. https://doi.org/10.1038/s41598-020-74215-5.

587 (29) Wu, A. N.; Biljecki, F. Roofpedia: Automatic Mapping of Green and Solar Roofs for an Open
588   Roofscape Registry and Evaluation of Urban Sustainability. *Landsc. Urban Plan.* **2021**, *214*.
589   https://doi.org/10.1016/J.LANDURBPLAN.2021.104167.

590 (30) Yu, J.; Wang, Z.; Majumdar, A.; Rajagopal, R. DeepSolar: A Machine Learning Framework to
591   Efficiently   Construct   a   Solar   Deployment   Database   in   the   United   States.   **2018**.
592   https://doi.org/10.1016/j.joule.2018.11.021.

593 (31) Parhar, P.; Sawasaki, R.; Nusaputra, N.; Vergara, F.; Todeschini, A.; Vahabi, H. HyperionSolarNet
594   Solar Panel Detection from Aerial Images.

595 (32) Kruitwagen, L.; Story, K. T.; Friedrich, J.; Byers, L.; Skillman, S.; Hepburn, C. A Global Inventory
596   of Photovoltaic Solar Energy Generating Units. *Nature* **2021**, *598* (7882), 604–610. https://doi.org/
597   10.1038/S41586-021-03957-7.

598 (33) Jordaan, S. M.; Heath, G. A.; Macknick, J.; Bush, B. W.; Mohammadi, E.; Ben-Horin, D.; Urrea,
599   V.; Marceau, D. Understanding the Life Cycle Surface Land Requirements of Natural Gas-Fired
600   Electricity. *Nat. Energy* **2017**, *2* (10), 804–812. https://doi.org/10.1038/s41560-017-0004-0.

601 (34) Dai, T.; Jordaan, S. M.; Wemhoff, A. P. Gaussian Process Regression as a Replicable, Streamlined
602   Approach to Inventory and Uncertainty Analysis in Life Cycle Assessment. *Environ. Sci. Technol.*
603   **2022**, *56* (6), 3821–3829. https://doi.org/10.1021/acs.est.1c04252.

604 (35) De Baan, L.; Mutel, C. L.; Curran, M.; Hellweg, S.; Koellner, T. Land Use in Life Cycle
605   Assessment: Global Characterization Factors Based on Regional and Global Potential Species
606   Extinction. *Environ. Sci. Technol.* **2013**, *47* (16), 9281–9290. https://doi.org/10.1021/es400592q.

91   23

92

94

(36)   Koellner, T.; Baan, L.; Beck, T.; Brandão, M.; Civit, B.; Margni, M.; Canals, L. M.; Saad, R.; Souza, D. M.; Müller-Wenk, R. UNEP-SETAC Guideline on Global Land Use Impact Assessment on Biodiversity and Ecosystem Services in LCA. *Int. J. Life Cycle Assess.* **2013**, *18* (6), 1188–1202. https://doi.org/10.1007/s11367-013-0579-z.

(37)   Hellweg, S.; Canals, L. M. I. Emerging Approaches, Challenges and Opportunities in Life Cycle Assessment. *Science (80-.).* **2014**, *344* (6188), 1109–1113. https://doi.org/10.1126/science.1248361.

(38)   Jordaan, S. M.; Combs, C.; Guenther, E. Life Cycle Assessment of Electricity Generation: A Systematic Review of Spatiotemporal Methods. *Adv. Appl. Energy* **2021**, *3* (July), 100058. https://doi.org/10.1016/j.adapen.2021.100058.

(39)   Cooney, G.; Jamieson, M.; Zaimes, G. G. *Development of an Open-Source Life Cycle Baseline for Electricity Consumption in the United States-LCAXIX*; National Energy Technology Laboratory (NETL), Pittsburgh, PA, Morgantown, WV …, 2019.

(40)   Cooney, G.; Skone, T. J.; Jamieson, M.; Zaimes, G. G. Open-Source Life Cycle Baseline for Electricity Consumption in the United States-LCI Public Release. In *AGU Fall Meeting Abstracts*; 2019; Vol. 2019, pp A41D-04.

(41)   Nelson, E.; Mendoza, G.; Regetz, J.; Polasky, S.; Tallis, H.; Cameron, D. R.; Chan, K. M. A.; Daily, G. C.; Goldstein, J.; Kareiva, P. M.; Lonsdorf, E.; Naidoo, R.; Ricketts, T. H.; Shaw, M. R. Modeling Multiple Ecosystem Services, Biodiversity Conservation, Commodity Production, and Tradeoffs at Landscape Scales. *Front. Ecol. Environ.* **2009**, *7* (1), 4–11. https://doi.org/10.1890/080023.

(42)   Jones, N. F.; Pejchar, L.; Kiesecker, J. M. The Energy Footprint: How Oil, Natural Gas, and Wind Energy Affect Land for Biodiversity and the Flow of Ecosystem Services. *Bioscience* **2015**, *65* (3), 290–301. https://doi.org/10.1093/biosci/biu224.

(43)   Jones, N. F.; Pejchar, L. Comparing the Ecological Impacts of Wind and Oil & Gas Development: A Landscape Scale Assessment. *PLoS One* **2013**, *8* (11). https://doi.org/10.1371/journal.pone.0081391.

(44)   Crooks, K. R.; Burdett, C. L.; Theobald, D. M.; King, S. R. B.; Di Marco, M.; Rondinini, C.; Boitani, L. Quantification of Habitat Fragmentation Reveals Extinction Risk in Terrestrial Mammals. *Proc. Natl. Acad. Sci. U. S. A.* **2017**, *114* (29), 7635–7640. https://doi.org/10.1073/pnas.1705769114.

(45)   The Western Electricity Coordinating Council (WECC). *2016 State of the Interconnection*; 2016.

(46)   U.S. Fish and Wildlife Service. ECOS: Environmental Conservation Online System https://ecos.fws.gov/ecp/ (accessed Jun 22, 2021).

(47)   Esri. World Topographic Map https://www.arcgis.com/home/item.html?id=7dc6cea0b1764a1f9af2e679f642f0f5.

(48)   Ronneberger, O.; Fischer, P.; Brox, T. U-Net: Convolutional Networks for Biomedical Image Segmentation. In *International Conference on Medical image computing and computer-assisted intervention*; Springer, 2015; pp 234–241.

95

96

97

98
646   (49)   Solórzano, J. V.; Mas, J. F.; Gao, Y.; Gallardo-Cruz, J. A. Land Use Land Cover Classification
647   with U-Net: Advantages of Combining Sentinel-1 and Sentinel-2 Imagery. *Remote Sens.* **2021**, *13*
648   (18), 3600. https://doi.org/10.3390/RS13183600/S1.

649   (50)   Zhang, W.; Tang, P.; Zhao, L. Fast and Accurate Land-Cover Classification on Medium-Resolution
650   Remote-Sensing Images Using Segmentation Models. *Int. J. Remote Sens.* **2021**, *42* (9), 3277–
651   3301. https://doi.org/10.1080/01431161.2020.1871094.

652   (51)   Sun, P.; Lu, Y.; Zhai, J. Mapping Land Cover Using a Developed U-Net Model with Weighted
653   Cross Entropy. https://doi.org/10.1080/10106049.2021.2017017.

654   (52)   Li, Y.; Zhou, Y.; Zhang, Y.; Zhong, L.; Wang, J.; Chen, J. DKDFN: Domain Knowledge-Guided
655   Deep Collaborative Fusion Network for Multimodal Unitemporal Remote Sensing Land Cover
656   Classification. *ISPRS J. Photogramm. Remote Sens.* **2022**, *186*, 170–189.
657   https://doi.org/10.1016/J.ISPRSJPRS.2022.02.013.

658   (53)   Wachs, E.; Engel, B. Land Use for United States Power Generation: A Critical Review of Existing
659   Metrics with Suggestions for Going Forward. *Renew. Sustain. Energy Rev.* **2021**, *143* (February).
660   https://doi.org/10.1016/j.rser.2021.110911.

661   (54)   Cagle, A. E.; Shepherd, M.; Grodsky, S. M.; Armstrong, A.; Jordaan, S. M.; Hernandez, R. R.
662   Standardized Metrics to Quantify Solar Energy-Land Relationships: A Global Systematic
663   Review . *Frontiers in Sustainability* . 2023.

664   (55)   Smil, V. Power Density Primer: Understanding the Spatial Dimension of the Unfolding Transition
665   to Renewable Electricity Generation (Part I-Definitions). **2010**.

666   (56)   Hernandez, R. R.; Hoffacker, M. K.; Field, C. B. Land-Use Efficiency of Big Solar. *Environ. Sci.*
667   *Technol.* **2014**, *48* (2), 1315–1323. https://doi.org/10.1021/es4043726.

668   (57)   U.S. Energy Information Administration. Form EIA-860 detailed data with previous form data
669   (EIA-860A/860B) https://www.eia.gov/electricity/data/eia860/ (accessed Nov 26, 2021).

670   (58)   Form   EIA-923   detailed   data   with   previous   form   data   (EIA-906/920)
671   https://www.eia.gov/electricity/data/eia923/ (accessed Nov 26, 2021).

672   (59)   Hamilton, S. D.; Millstein, D.; Bolinger, M.; Wiser, R.; Jeong, S. How Does Wind Project
673   Performance Change with Age in the United States? *Joule* **2020**, *4* (5), 1004–1020.
674   https://doi.org/10.1016/j.joule.2020.04.005.

675   (60)   Chomphosy, W. H.; Varriano, S.; Lefler, L. H.; Nallur, V.; McClung, M. R.; Moran, M. D.
676   Ecosystem Services Benefits from the Restoration of Non-Producing US Oil and Gas Lands. *Nat.*
677   *Sustain.* **2021**, *4* (6), 547–554. https://doi.org/10.1038/s41893-021-00689-4.

678   (61)   Johnson, N.; Gagnolet, T.; Ralls, R.; Stevens, J. *Natural Gas Pipelines. Excerpt from Report 2 of*
679   *the Pennsylvania Energy Impacts Assessment*; 2011.

680   (62)   Palmer-Wilson, K.; Donald, J.; Robertson, B.; Lyseng, B.; Keller, V.; Fowler, M.; Wade, C.;
681   Scholtysik, S.; Wild, P.; Rowe, A. Impact of Land Requirements on Electricity System
682   Decarbonisation   Pathways.   *Energy   Policy* **2019**, *129* (January), 193–205.
683   https://doi.org/10.1016/j.enpol.2019.01.071.

99   25

100

101

102
684

104